

Direction Matters: Learning Force Direction Enables Sim-to-Real Contact-Rich Manipulation

Yifei Yang¹, Anzhe Chen¹, Zhenjie Zhu¹, Kechun Xu¹, Yunxuan Mao¹, Yufei Wei¹,
Lu Chen², Rong Xiong^{1,2}, Yue Wang¹

¹ Zhejiang University ² Zhejiang Humanoid Robot Innovation Center

Abstract—Sim-to-real transfer for contact-rich manipulation remains challenging due to the inherent discrepancy in contact dynamics. While existing methods often rely on costly real-world data or utilize blind compliance through fixed controllers, we propose a framework that leverages expert-designed controller logic for transfer. Inspired by the success of privileged supervision in kinematic tasks, we employ a human-designed finite state machine based position/force controller in simulation to provide privileged guidance. The resulting policy is trained to predict the end-effector pose, contact state, and crucially the desired contact force direction. Unlike force magnitudes, which are highly sensitive to simulation inaccuracies, force directions encode high-level task geometry and remain robust across the sim-to-real gap. At deployment, these predictions configure a force-aware admittance controller. By combining the policy’s directional intent with a constant, low-cost manually tuned force magnitude, the system generates adaptive, task-aligned compliance. This tuning is lightweight, typically requiring only a single scalar per contact state. We provide theoretical analysis for stability and robustness to disturbances. Experiments on four real-world tasks, i.e., microwave opening, peg-in-hole, whiteboard wiping, and door opening, demonstrate that our approach significantly outperforms strong baselines in both success rate and robustness. Videos are available at: <https://yifei-y.github.io/project-pages/DirectionMatters/>.

I. INTRODUCTION

Simulation has revolutionized robotic learning by providing a scalable, safe, and cost-effective environment for large-scale data generation [21, 23, 5, 9]. While this paradigm has propelled advancements in kinematic-centric tasks such as pick-and-place [20, 8, 14], extending these capabilities to contact-rich manipulation remains a challenge. The primary obstacle is the gap in modeling contact dynamics between simulated and real environments. Consequently, policies trained in simulation tend to overfit to these inaccuracies. When deployed to the real world, this discrepancy leads the robot to execute actions that violate real-world physical constraints, resulting in dangerous interaction, task failure and even hardware damage.

To address the challenge of contact-rich manipulation, current research generally falls into two paradigms, as shown in Figure 1. The first discards the simulation and relies entirely on *real-world data collection* [11, 31, 18], which intrinsically bypasses the dynamics gap. However, the extra cost of data acquisition restricts the scalability of such methods. The second paradigm combines simulation-trained position policies with real-world compliant controllers [33, 15, 17]. While this approach leverages the diversity of simulation data, it suffers from a limitation: *blind compliance*. Since these policies

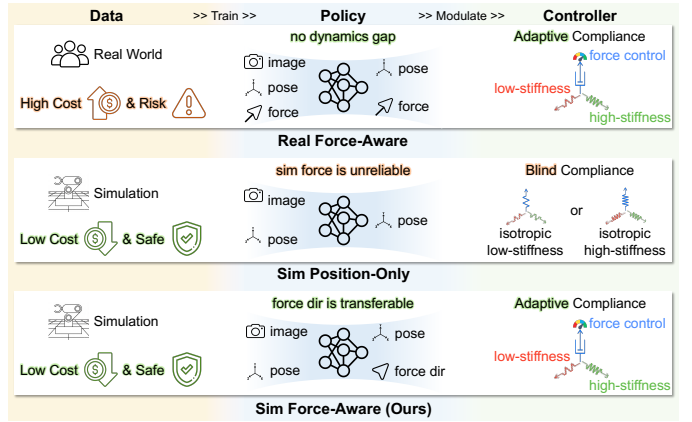


Fig. 1. Compared to existing paradigms, our framework identifies force direction as a transferable signal that specifies task-relevant interaction intent and can be reliably learned in simulation, enabling force-aware policy training with pure simulation data and adaptive compliance in the real world.

typically predict only end-effector poses, the downstream controller is specified with conservative, isotropic settings, passively accommodating errors rather than actively managing the interaction. This motivates a fundamental question: *Can we harness the scalability of simulation while enabling intelligent, task-aware compliance in the real world?*

Our key insight stems from the mechanism of successful sim-to-real transfer in kinematic tasks, where policies mimic privileged expert behavior to act as high-level operators for low-level position controllers. For contact-rich tasks, human experts typically design Finite State Machines (FSMs) that switch between position and force controller based on task phases. We adopt this philosophy by using such an expert FSM in simulation to provide privileged supervision, training a policy to output state-switching signals and controller parameters. However, not all controller parameters transfer equally. Direct prediction of force magnitudes or stiffness profiles is fragile, as these values are coupled with simulated contact dynamics. To address this, we identify a crucial invariance: while force magnitude is sensitive to the dynamics gap, the *target contact force direction* is primarily constrained by task geometry and remains robust across domains.

Building on the analysis above, we propose a framework for sim-to-real contact-rich manipulation. We formulate the policy to predict the contact force direction and the contact state alongside end-effector poses, which allows the policy to be trained exclusively on large-scale simulation data with hu-

man designed privilege supervision, bypassing the high costs and safety risks of real-world data collection. For real-world execution, we propose a force-aware admittance controller that combines the policy predictions with a human-specified target force magnitude. Because this magnitude is typically constant per contact phase, manual tuning is lightweight, often requiring only a single scalar per task. The resulting controller achieves adaptive compliance that aligns with high-level task intent while rejecting external disturbances. Furthermore, we provide a theoretical analysis on the controller stability with and without disturbance. To validate our framework, we conducted extensive real-world experiments on four contact-rich tasks: microwave opening, peg-in-hole, whiteboard wiping, and door opening. These tasks represent a broad spectrum of interaction constraints and force requirements. Our method consistently demonstrates effective performance in terms of both task success rates and robustness. In summary, our main contributions are as follows:

- A novel framework that leverages pure simulation data and lightweight manual tuning to solve complex real-world contact-rich manipulation tasks.
- A policy action formulation to generate the force direction and contact state, which is invariant to dynamics gap between simulation and real world.
- An admittance controller with adaptive compliance specified by the policy force predictions, and further analyzed for stability.
- Extensive real-world experiments validate the superiority and robustness of the proposed approach on diverse contact-rich tasks.

II. RELATED WORK

A. Real-World Learning for Contact-Rich Manipulation

Contact-rich manipulation is essential for many real-world robotic applications, such as assembly, articulated object operation, and surface interaction, where success critically depends on applying appropriate forces rather than merely reaching geometric targets. Learning directly in the real world is therefore highly appealing, as it provides access to accurate physical interactions and naturally captures complex contact dynamics without relying on explicit modeling.

One prominent line of work adopts imitation learning from human demonstrations. Among them, some focus on predicting desired force [18] or stiffness profiles [11, 1, 6] explicitly, while others [31, 10, 36, 35] generate reference poses that are executed by fixed compliant controllers, achieving implicit force regulation. In addition, CR-DAgger [29] trains a residual policy to predict force-aware corrective actions for position-only policies via human-in-the-loop interaction.

Another line of research employs real-world reinforcement learning [19, 16, 12, 28], which optimizes policies through trial-and-error interaction in the real environment. This paradigm is powerful as it can in principle, discover sophisticated contact strategies beyond human demonstrations.

Despite their effectiveness, they require extensive real-world interaction to acquire force-related supervision. Collecting

such data is time-consuming and labor-intensive. More critically, contact-rich interactions inherently pose safety risks, which severely constrain scalability.

B. Sim-to-Real Transfer for Contact-Rich Manipulation

To alleviate the cost and safety concerns of real-world learning, extensive prior work studies sim-to-real transfer for contact-rich manipulation, aiming to exploit the scalability of simulation. A key challenge lies in the mismatch of contact dynamics between simulation and reality, which makes force-related behaviors particularly difficult to transfer.

One line of research focuses on system identification and dynamics parameter alignment [3, 30, 22], calibrating simulators to better match real-world contact properties. While improved fidelity can facilitate transfer, accurately identifying contact parameters is often task- and object-specific and requires substantial real-world interaction or manual tuning.

Another approach augments simulation training with limited real data using residual learning or policy finetuning [26, 27, 34, 13]. Though effective, these hybrid methods undermine the scalability and safety benefits of pure simulation.

A third paradigm applies reinforcement learning with dynamics randomization [32, 7, 24] to enable zero-shot transfer. Despite promising results, this strategy demands careful engineering of randomization distributions and rewards. Moreover, reinforcement learning is inherently data-inefficient. In this settings, the additional need to cope with varying and uncertain contact dynamics further increases the learning burden.

Finally, some methods combine simulation-trained, position-only policies with compliant controllers in the real world [33, 15, 17]. While this avoids explicit force prediction and improves safety, manually specified and isotropic compliance often leads to blind compliance and limited task effectiveness.

In summary, existing approaches mitigate the dynamics gap via parameter alignment, real-world adaptation, dynamics randomization, or passive compliance, but do so at the expense of scalability, safety, data efficiency, or task effectiveness.

III. PROBLEM ANALYSIS

This section analyzes the structure requirements for contact-rich manipulation and derives the design principles that motivate our approach. We first characterize the ideal policy for contact-rich tasks as a Finite State Machine (FSM) that modulates control modes and reference signals based on contact state (Section III-A). We then identify the dynamics gap as the primary impediment to learning reference forces in simulation (Section III-B). Finally, we isolate force directions as dynamics-invariant quantities that can be robustly learned in simulation, laying the theoretical foundation for our framework (Section III-C).

A. Finite State Machine for Contact-Rich Tasks

The policy for kinematic tasks typically functions as a high-level planner, generating reference pose trajectories that are realized by a low-level position controller with manually

tuned gains. This allows the policy to focus on “where to go” (geometry) while relying on the controller to handle “how to move” (dynamics). We posit that a similar hierarchy can be applied to contact-rich tasks.

However, contact-rich manipulation inherently involves dynamic transitions, and reference poses alone are insufficient to fully specify the desired behavior during contact. An effective policy therefore naturally operates as a Finite State Machine (FSM), dynamically switching control modes and reference modalities according to the contact state. In the *Free Motion* phase, where external constraints are absent, the FSM behaves similarly to a kinematic policy by generating reference poses and operating the controller in position control mode. In contrast, during *Contact Interaction*, once the robot engages with the environment, the objective shifts from “where to go” to “how much force to exert at which location”, requiring the FSM to output force references alongside poses and to switch the controller to a hybrid position/force control mode to achieve the desired pose-force behavior.

This analysis highlights that contact-rich tasks require policy to predict contact states and reference force besides poses.

B. Sim-Real Gap Analysis

The discrepancies between simulation and reality can be categorized into visual and dynamic gaps. While both contribute to transfer failure, they affect the robotic system through fundamentally different mechanisms.

The Visual Gap arises from differences in rendering, lighting, and texture. For a policy, this primarily affect state estimation, for instance, misinterpreting the handle’s pose due to specular reflections. However, this challenge has been extensively studied, and techniques such as domain randomization and realistic rendering have largely mitigated its impact.

The Dynamics Gap stems from discrepancies in dynamics model and physical parameters. This results in a significant large mismatch in contact-induced force-motion responses during robot-object interaction between simulation and reality. Therefore, the dynamics gap is the primary bottleneck in approaching contact-rich tasks through simulation.

C. Invariance Analysis

The previous analysis reveals a contradiction: the policy for contact-rich tasks must predict reference forces, yet force prediction learned in simulation is fragile due to the dynamics gap. To resolve this, we analyze the structure of interaction forces to identify components that are robust to dynamics gap.

We focus on translational interaction forces ($F \in \mathbb{R}^3$), as they are the primary drivers for overcoming resistance or maintaining contact in our selected scenarios. During contact, the robot’s end-effector motion is constrained to a manifold imposed by the object’s mechanical and geometric structure. This constraint induces a natural decomposition of the interaction force into orthogonal subspaces defined by the manifold:

- *Tangent Space (F_t)*: Forces lying in the tangent space of contact manifold, aligning with feasible motion directions.
- *Normal Space (F_n)*: Forces orthogonal to the manifold, arise from geometric constraints restricting motion. The role of F_n is task-dependent: for tasks requiring sustained contact (e.g., whiteboard wiping), it provides necessary pressure; for kinematically constrained tasks (e.g., door opening), it represents constraint forces that should be minimized.

The tangent forces arise from dynamics-dependent resistance such as friction or damper and the normal forces are induced by the contact dynamics at the robot-object interface. Therefore, F_t and F_n are correlated with the dynamics. However, their *directions*, $\mathbf{t} = \frac{F_t}{\|F_t\|}$ and $\mathbf{n} = \frac{F_n}{\|F_n\|}$, are determined by the manifold, i.e. task geometry, which is unrelated to dynamics. Specifically, the tangent force direction \mathbf{t} aligns with the feasible motion direction, and the normal force direction \mathbf{n} aligns with the surface normal vector at the contact point. The ground-truth force directions in simulation provide robust, dynamics-invariant supervision signals for policy learning.

In addition, the contact state used to trigger FSM switches is also a geometric property, depending on the relative distance between the end-effector and the object surface.

This analysis motivates our proposed framework. Rather than learning the unreliable reference force, we restrict the policy to predict dynamics-invariant force directions and contact state, while leaving the force magnitude to be manually specified at deployment, which is typically constant within each contact phase. Thus, the policy can be trained in simulation and transfer to the real world with minor manual tuning.

IV. POLICY FORMULATION AND LEARNING

Building on the analysis in Section III, we introduce a novel policy formulation that imitates the FSM to predict the contact state and reference signals, while explicitly avoiding reliance on inaccurate simulation dynamics (Section IV-A). We then describe an automatic data generation pipeline that exploits privileged simulation information to efficiently produce diverse demonstrations (Section IV-B). Finally, we detail the policy architecture and learning procedure (Section IV-C). The overall framework is illustrated in Figure 2.

A. Policy Formulation

Contact-rich manipulation necessitates the policy to predict not only the reference poses but also the reference forces and contact states, acting as a FSM to switch between different control modes and modulate controller behavior. However, to enable sim-to-real transfer, it is crucial to decouple the policy from the dynamics. Guided by the invariance analysis in Section III-C, we propose a dynamics-invariant policy formulation which predicts the contact state and force direction alongside the kinematic trajectory.

We formulate the policy to map the current observation O_t , which includes RGB images and proprioception, to a sequence of h future actions $\{A_{t+k}\}_{k=0}^{h-1}$. This action chunking strategy encourages temporal consistency in predictions. The detailed observation specification is provided in Appendix A. The predicted action at each step (A_t) is defined as a tuple of three components:

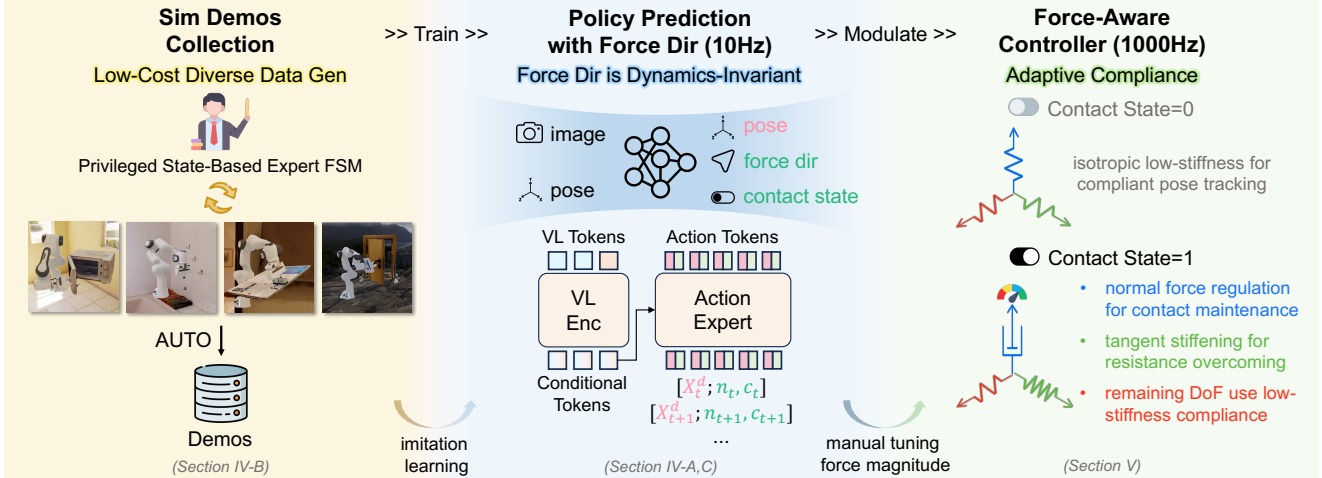


Fig. 2. Overview of the proposed framework. (Left) In simulation, we implement an expert Finite State Machine based on privileged state to generate diverse demonstrations. (Middle) Identifying force direction and contact state as dynamics-invariant quantities that encode task intent, the policy is trained to predict these signals alongside poses using simulation data. (Right) In the real world, the policy outputs configure a force-aware admittance controller, which combines the predicted force direction with a manually specified magnitude to achieve adaptive, task-aligned compliance.

- Reference Pose and Gripper Command ($X_t^d \in \mathbb{R}^{10}$): A vector containing the end-effector position (3), the 6D rotation (6) proposed in [37], and the gripper command (1).
- Normal Force Direction ($n_t \in \mathbb{R}^3$)
- Contact State ($c_t \in \{0, 1\}$): A binary indicator predicting whether the end-effector is in contact with the object.

Note that we do not explicitly predict the tangent force direction t , as it can be derived from the predicted reference position and the normal force direction via Eq. 5. For simplicity, we omit the subscript t when no ambiguity arises.

B. Demonstrations Generation

To train our proposed policy, we utilize privileged information in simulation to construct expert FSMs for each task, generating large-scale demonstrations.

As illustrated in Section III-A, the FSM should employ distinct strategies in different contact states. In *Free Motion* phases, such as approaching the object or retracting after task completion, the expert FSM generates pose trajectories toward manually defined object-centric key poses using linear interpolation. In *Contact Interaction* phases, feasible motion is constrained by task geometry and articulation mechanisms, and the FSM follows human-designed kinematic rules tailored to each task (details provided in Appendix B).

Ideally, the FSM should adapt control modes based on contact state. However, we adopt a simplified design that uses a high-stiffness pose-tracking controller throughout, as privileged state enables near-perfect trajectories and safety constraints are absent. This simplification reduces the complexity of expert design and does not compromise data quality.

Based on the expert FSM, we extract supervision signals that align with the proposed action space. The reference pose at time t is supervised using the end-effector pose at time $t+1$ to avoid coupling with dynamics. The gripper command is directly taken from the expert command at time t . The normal force direction is obtained from the normal of the contact manifold at time $t+1$. Finally, the contact state is provided

by the expert FSM according to its phase segmentation.

The details of simulation environment setup and randomization strategy are provided in Appendix C and D.

C. Network Architecture and Training

We instantiate our policy using E2VLA [4], due to its strong 3D geometric reasoning capabilities. By aligning visual representations and action tokens with the underlying 3D physical space, E2VLA enables more accurate spatial inference.

1) *Architecture Modification*: To accommodate our expanded action formulation, we modify the diffusion action expert of E2VLA by extending the input and output projection layers. This parameter-efficient change enables joint prediction of reference poses, normal force directions, and contact states within a unified generative framework. The details of finetuning strategy are provided in Appendix F.

2) *Loss Function*: The network is trained with loss:

$$\mathcal{L} = \lambda_1 \|X^d - \hat{X}^d\|_1 + \lambda_2 \|\mathbf{n} - \hat{\mathbf{n}}\|_1 + \lambda_3 \|c - \hat{c}\|_1, \quad (1)$$

where \hat{X}^d denotes the ground-truth reference pose and gripper command; $\hat{\mathbf{n}}$ and \hat{c} represent the ground-truth normal force direction and contact state, respectively. The hyperparameters $\lambda_{1,2,3}$ balance the different objectives.

V. FORCE-AWARE ADMITTANCE CONTROL

The policy introduced in Section IV acts as a high-level FSM, predicting contact states and reference signals to modulate the controller behavior. In this section, we present a force-aware admittance controller that integrates these predictions with a small set of manually specified scalar parameters to achieve adaptive compliance during interaction (Section V-A). We further provide a stability analysis of the normal-direction dynamics under different contact conditions (Section V-B).

A. Controller Formulation

We employ a Cartesian admittance controller with translational dynamics

$$M\ddot{\mathbf{x}}_r + D\dot{\mathbf{x}}_r + K(\mathbf{x}_r - \mathbf{x}_{cmd}) = F_{ext} - F_{cmd}, \quad (2)$$

where \mathbf{x}_r denotes the compliant reference position computed by the admittance law. Assuming a sufficiently high-bandwidth low-level position controller, the actual end-effector position is approximated by \mathbf{x}_r in the following analysis.

An analogous admittance formulation is applied in the rotational space, where the policy provides commanded orientations and the commanded torque is set to zero.

The matrices M , D , and K are diagonal with identical (m, d, k) along each axis. The same low-stiffness, over-damped parameters are used across all tasks without task-specific tuning; parameter selection principles are summarized in Appendix E. Rotational gains follow the same design principles with proportionally smaller values.

1) *Normal Force Regulation*: The commanded position is directly taken from the policy prediction, i.e., $\mathbf{x}_{cmd} = \mathbf{x}^d$, where $\mathbf{x}^d \in \mathbb{R}^3$ denotes the translational component of the predicted reference pose X^d . The commanded force F_{cmd} is set to zero when the predicted contact state $c = 0$, resulting in standard admittance-based compliant pose tracking. When $c = 1$, the commanded force is applied along the predicted normal direction \mathbf{n} as $F_{cmd} = f\mathbf{n}$, where

$$f = f_H + \mathbf{n} \cdot K(\mathbf{x}_{cmd} - \mathbf{x}_r) + \mathbf{n} \cdot D\dot{\mathbf{x}}_r. \quad (3)$$

The second term compensates for the spring force induced by the position error along \mathbf{n} , while the third term penalizes velocity. This yields damping control along \mathbf{n} :

$$m\ddot{x}_n + 2d\dot{x}_n = f_{ext,n} - f_H, \quad (4)$$

where \ddot{x}_n , \dot{x}_n , and $f_{ext,n}$ denote the acceleration, velocity, and external force along \mathbf{n} , respectively. This drives the robot to steadily establish and maintain contact with the target force magnitude f_H , a task-specific manually tuned scalar. For tasks where contact is primarily maintained by the gripper closure (e.g., microwave opening), normal force regulation is unnecessary. In these cases, we simply set $F_{cmd} = \mathbf{0}$ and rely on pose tracking together with the gripper to sustain contact.

2) *Tangent Stiffening*: For tasks that require overcoming resistive forces, the stiffness along the tangent direction is increased to provide additional assistance during contact. The tangent direction \mathbf{t} is obtained by projecting the motion direction \mathbf{v} onto the subspace orthogonal to \mathbf{n} :

$$\mathbf{t} = \frac{(I - \mathbf{n}\mathbf{n}^\top)\mathbf{v}}{\|(I - \mathbf{n}\mathbf{n}^\top)\mathbf{v}\|}, \quad (5)$$

where $\mathbf{v} = (\mathbf{x}_{cmd} - \mathbf{x}_r)/\|\mathbf{x}_{cmd} - \mathbf{x}_r\|$. Along \mathbf{t} , the translational stiffness is scaled by a multiplicative factor, and the corresponding damping is updated according to the same over-damped formulation. Whether tangent stiffening is enabled is a task-dependent binary parameter specified at deployment. The scaling factor can also be adjusted, but in our experiments, a value of four sufficed across all tasks, consistent with the stiffness ratios used in the baselines.

The controller selectively regulates normal contact and tangent assistance while maintaining low-stiffness admittance elsewhere. This mechanism achieves adaptive compliance that is task-effective and robust during contact-rich interactions.

B. Stability Analysis

To characterize the safety and robustness properties of the proposed controller, we analyze the stability of the normal-direction dynamics in Eq. 4 under different contact conditions.

We model the environment as a linear spring with stiffness k_e and denote the rest point of the environment as x_e . The external force can then be expressed as

$$f_{ext,n} = k_e(x_e - x_n), \quad (6)$$

where x_n is the robot position along the normal direction n .

we present three propositions characterizing the stability properties of the closed-loop normal-direction dynamics. The detailed proofs are provided in the Appendix G.

- **Proposition 1:** *Under disturbance-free conditions, the closed-loop normal-direction dynamics is asymptotically stable and converges to the equilibrium point $x_n = x_e - f_H/k_e$ such that $f_{ext,n} = f_H$.*
- **Proposition 2:** *When contact with the environment is lost due to an external disturbance (e.g., lowering the whiteboard during wiping), the closed-loop normal-direction dynamics are asymptotically stable in velocity. Specifically, the end-effector velocity converges to the steady-state value $\dot{x}_n = -\frac{f_H}{2d}$, which drives the robot toward the environment to facilitate contact re-establishment.*
- **Proposition 3:** *When the disturbance occurs during contact, the closed-loop normal-direction dynamics is input-to-state stable (ISS) with respect to the disturbance.*

Propositions 1–3 establish that our normal-direction controller is stable across all contact states. Specifically, it guarantees asymptotic convergence to the target force magnitude during interaction, ensures stable approaching behavior upon contact loss, and maintains bounded errors under external disturbances. For all other degrees of freedom, the system reduces to a standard admittance formulation, with stability following from classical over-damped dynamics analysis.

VI. EXPERIMENTS

A. Setup

1) *Hardware*: We conduct experiments on a Franka robot arm equipped with a Franka Hand gripper. The robot is outfitted with a wrist-mounted camera and 2 (2 for whiteboard wiping, 1 for other tasks) fixed third-view cameras to provide RGB images. More details are provided in Appendix H.

2) *Baselines*: We compare our approach against position-only policies integrated with blind compliance controllers:

- **Finetuned π_0 + Admittance controller:** Finetune π_0 [2] with the same data as our method, and deploy it with three different but blind stiffness settings (low / mid / high) in the admittance controller.
- **Finetuned E2VLA + Admittance controller:** Finetune E2VLA [4] with the same data as our method, and deploy it with three different but blind stiffness settings (low / mid / high) in the admittance controller.

Rotational admittance is fixed at low stiffness, while translational stiffness for mid- and high-stiffness baselines is scaled



Fig. 3. The involved objects for four contact-rich manipulation tasks.

by $4\times$ and $16\times$ respectively. Our controller utilizes the baseline low-stiffness translational setting, with a $4\times$ scale applied for tangent stiffening. To ensure comparable stability, all damping parameters are adjusted using the same over-damped formulation.

3) *Tasks*: We evaluate our framework on four contact-rich tasks in the real world: Microwave Opening (MO), Peg-in-Hole (PH), Whiteboard Wiping (WW), Door Opening (DO). The objects involved in each task are illustrated in Figure 3. These tasks cover a wide spectrum of contact scenarios, encompassing diverse contact dynamics, geometric constraints, and interaction complexities as shown in Table I. The detailed task descriptions are provided in Appendix I.

4) *Evaluation Protocols*: For each task and method, we execute 25 real-world rollouts with randomized object and robot initial poses. We use similar initial states across all methods to ensure fair comparisons. A trial is deemed successful if the robot completes the task within a predefined time limit without triggering safety stops. For the detailed definition of object pose randomization, disturbance protocols and success criteria, please see Appendix J.

To evaluate robustness, disturbances are applied to 5 trials that successfully establish initial contact. Initial contact is task-specifically defined: grasping handles (MO and DO), partial peg insertion (PH), or eraser-whiteboard engagement (WW). To ensure consistency, we pre-select 5 initial configurations with a high likelihood of contact. If a model fails the initial contact in a selected trial, we substitute it with next successful rollout from the remaining set to ensure the disturbance phase is reached. This protocol decouples robustness evaluation from initial contact success, focusing on the model’s ability to maintain and adapt contact under disturbances.

5) *Implementation Details*: Whether to enable normal force regulation and tangent stiffening, as well as the corresponding target normal force magnitude are specified per task as described in Table I. Note that the target normal force magnitude is set to be constant, where the manual tuning can be minimal. More implementation details are provided in Appendix K.

B. Comparison Study

1) *Success and Robustness*: Table II summarizes success rates across four tasks under undisturbed (SR-ND) and disturbed (SR-D). Our method achieves a 91% overall success rate, outperforming the best baseline (67%). In resistance-heavy tasks (MO and DO), baselines improve performance via higher stiffness but suffer under disturbances due to reduced compliance. Our approach avoids this trade-off by selectively providing assistance along task-relevant directions. For contact-maintenance tasks (PH and WW), pure stiffness-based control fails to regulate force reliably; our explicit normal force

TABLE I
TASK CHARACTERISTICS AND REQUIREMENTS.

	Constraint Switching	Resistance Overcoming (Tangent Stiffening)	Contact Maintenance (Normal Force Regulation)	Target Normal Force Magnitude (N)
MO	×	✓	✗	-
PH	×	✗	✓	2
WW	×	✓	✓	4
DO	✓	✓	✗	-

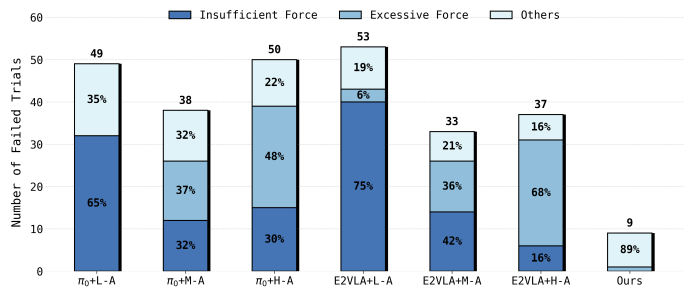


Fig. 4. Failure Mode Statistics. Baselines suffer from a high number and proportion of force-related failures, while our method significantly reduces both insufficient- and excessive-force failures.

control ensures robust contact. Note that higher SR-D than SR-ND in some models result from the evaluation protocol (Section VI-A4), where disturbances applied to successful initial trajectories occasionally bias outcomes toward success if safety limits are not triggered.

2) *Failure Analysis*: Failures are categorized into: (1) Insufficient Force (failed resistance/contact), (2) Excessive Force (safety stops), and (3) Others (geometric/grasping errors). Fig. 4 displays the distribution of these modes, with bar heights showing absolute counts and percentages showing relative proportions. While baselines are dominated by force-related failures, our method reduces both Insufficient and Excessive Force modes, validating our adaptive compliance strategy. “Other” failures, primarily due to visual out-of-distribution (OOD) inputs, remain comparable between our framework and the position-only E2VLA baseline, as both share the same pre-trained model.

3) *Task Completion Quality*: Table III presents the average insertion depth (PH) and remaining ink length (WW) for successful trials, serving as metrics for execution quality. Beyond superior success rates, our approach consistently achieves higher-quality outcomes, i.e. deeper insertions and more thorough wiping. These results indicate that our framework facilitates more precise and consistent contact interactions. For MO and DO, once the initial lock is released, hinge resistance is low, hence all successful methods achieve comparable opening angles regardless of stiffness variations.

C. Ablation Study

We conduct ablation studies on the whiteboard wiping (Table IV). The higher SR-D compared to SR-ND are explained by the evaluation protocol bias discussed in Section VI-B.

1) *Effectiveness of Finetuning*: Finetuning pre-trained VLA (No.7) outperforms training from scratch (No.1) in both success rate and execution quality, confirming that our strategy

TABLE II
TASK SUCCESS RATES COMPARISON.
SR-ND: SUCCESS RATE WITHOUT DISTURBANCE; SR-D: SUCCESS RATE WITH DISTURBANCE; SR: OVERALL SUCCESS RATE.

	Microwave Opening			Peg-in-Hole			Whiteboard Wiping			Door Opening			Overall		
	SR-ND (%)	SR-D (%)	SR (%)	SR-ND (%)	SR-D (%)	SR (%)	SR-ND (%)	SR-D (%)	SR (%)	SR-ND (%)	SR-D (%)	SR (%)	SR-ND (%)	SR-D (%)	SR (%)
π_0+L-A	30	60	36	35	80	44	35	60	40	80	100	84	45	75	51
π_0+M-A	75	60	72	30	60	36	60	60	60	90	40	80	64	55	62
π_0+H-A	60	40	56	35	20	32	45	20	40	80	40	72	55	30	50
E2VLA+L-A	15	40	20	55	100	64	30	60	36	65	80	68	41	70	47
E2VLA+M-A	90	20	76	55	60	56	55	80	60	85	40	76	71	50	67
E2VLA+H-A	70	20	60	70	40	64	65	40	60	75	40	68	70	35	63
Ours	100	100	100	75	100	80	95	100	96	90	80	88	90	95	91

TABLE III
TASK COMPLETION QUALITY COMPARISON.

	Peg-in-Hole Insertion Depth (mm) \uparrow	Whiteboard Wiping Remain Ink Length (cm) \downarrow
π_0+L-A	21.5	2.3
π_0+M-A	21.3	2.8
π_0+H-A	22.8	1.3
E2VLA+L-A	21.9	2.0
E2VLA+M-A	23.6	1.1
E2VLA+H-A	21.0	0.8
Ours	25.0	0.8

successfully leverages pre-trained priors. However, comparing No.4-6 against their counterparts in Tables II and III (E2VLA+L-A/M-A/H-A) reveals a slight performance drop when force direction and contact state losses are added. This suggests introducing extra action dimensions may marginally compromise pose prediction accuracy, highlighting a trade-off when extending pre-trained VLAs with new modalities.

2) *Effectiveness of Force-aware Controller*: Despite the lack of pre-training, No.1 outperforms No.4-6, which are finetuned from pre-trained models but use standard admittance controllers to track the predicted poses. This result highlights that, for contact-rich manipulation tasks, force-related constraints play a critical role, and large-scale pose-only pre-training alone may be insufficient. Synergy of policy and controller is a critical aspect that require careful consideration.

3) *Effectiveness of Normal Force Regulation*: Comparing No.2 with No.7 reveals that removing normal force regulation results in a substantial drop in success rate. Without explicit regulation of the normal contact force, the robot struggles to maintain stable contact, leading to unreliable task execution. A similar trend is observed when comparing No.3 and No.4.

4) *Effectiveness of Tangent Stiffening*: While normal force ensures the task is feasible, tangent stiffening determines how well it is executed. Comparing to No.3, No.7, augmented with tangent stiffening, exhibits a significantly shorter remaining ink length. Without tangent stiffening, the robot often suffers from large tangent tracking errors due to friction between the eraser and the whiteboard, resulting in poor wiping quality. Comparing No.2 and No.4 also supports this observation.

5) *Effectiveness of Adaptive Compliance*: Comparisons between No.4-6 and No.7 highlight the superiority of our framework. Pure pose prediction combined with isotropic compliance control (No.4-6) faces a dilemma: low stiffness is safe

TABLE IV
ABLATION STUDY ON WHITEBOARD WIPING TASK.

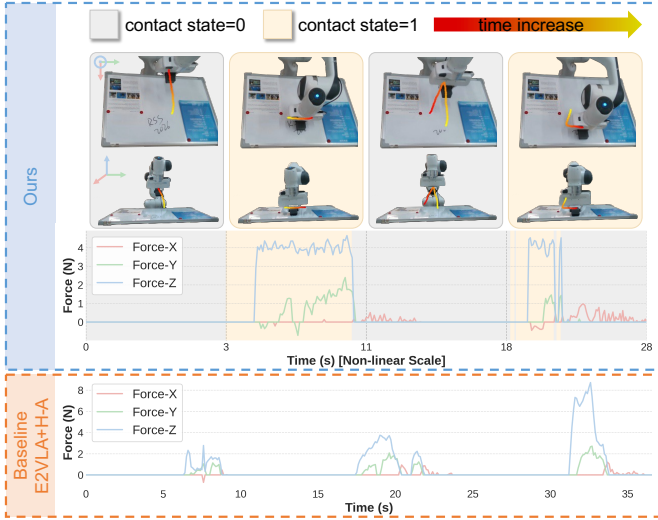
No.	Pre Train	Normal Force Regulation	Tangent Stiffening	SR-ND (%) \uparrow	SR-D (%) \uparrow	SR (%) \uparrow	Remain Ink Length (cm) \downarrow
1	\times	✓	✓	75	80	76	2.7
2	✓	✗	✓	30	80	40	1.7
3	✓	✓	✗	75	80	76	3.7
4	✓		L-A	30	80	40	3.5
5	✓		M-A	40	80	48	2.4
6	✓		H-A	40	40	40	1.8
7	✓	✓	✓	95	100	96	0.8

but ineffective, while high stiffness improves task execution quality but becomes brittle under disturbances. Moreover, increasing stiffness cannot ensure contact maintenance, as evidenced by the low success rates of No.4-6. In contrast, our framework resolves this trade-off by adaptively modulating compliance and explicitly regulating task-relevant forces, achieving high success rates and robustness to disturbances while maintaining high execution quality.

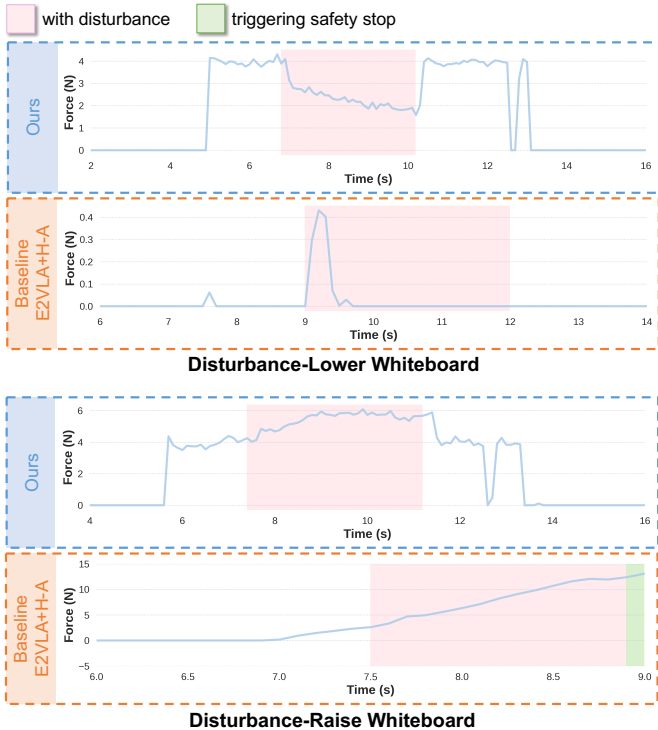
D. Case Study

1) *Contact Force Stabilization*: As illustrated in Fig. 5a, during whiteboard wiping, our normal contact force (Force-Z) converges to the target force magnitude 4N immediately upon contact (yellow region), whereas the baseline fluctuates. During height perturbations (Fig. 5b), our method robustly adapts to surface displacement: when the board is lowered (top), it tracks the downward motion and the force re-converges to the target once the height stabilizes; when the board is raised (bottom), the force remains bounded without safety-limit violations and similarly returns to the target after height stabilization. In contrast, the baseline loses contact when lowering and triggers safety stops when raising. These results empirically validate the stability analysis in Section V-B.

2) *Interaction with Tangent Stiffening*: Fig. 6a demonstrates our method’s adaptive stiffness during microwave opening. Upon encountering snap-lock resistance, tangent stiffness (Stiffness-Y, green) increases to generate sufficient force (Force-Y, green). As the door swings, the stiffening direction shifts gradually from the y to the x -axis. Fig. 6b shows that our method maintains bounded forces under disturbances, ensuring safety. In contrast, the low-stiffness baseline (Fig. 6a bottom) fails to overcome the lock, while the mid-stiffness baseline



(a) Top: forces of our method, where the yellow region indicates time steps with predicted contact state = 1 and the trajectories are visualized above. Bottom: forces of the baseline with highest SR-ND under a comparable setting.



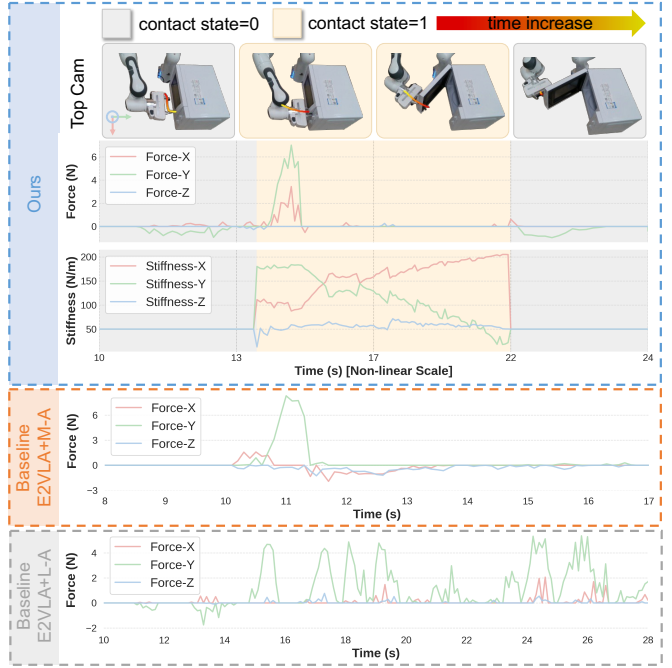
(b) Z-axis forces are shown for board lowering and lifting disturbance. The red region indicates the time that the disturbance is applied, while the green region denotes robot safety stops triggered by force-limit violations.

Fig. 5. Force response during whiteboard wiping under nominal conditions (a) and height disturbances (b).

(Fig. 6a middle), though capable of opening the door, triggers safety stops due to force-limit violations under disturbance (Fig. 6b bottom, green region).

E. Limitations

There are two primary avenues for future research. First, the current formulation focuses on translational forces; extending



(a) Top: force and stiffness variation of our method, where the yellow region indicates time steps with predicted contact state = 1. Middle & Bottom: force variation of baselines with highest and lowest SR-ND.



(b) Force variation under disturbances. The red region indicates the time that the disturbance is applied; the green region denotes robot safety stops triggered by force-limit violations; the purple region marks the moment that the door lock is pulled open.

Fig. 6. Force response during microwave opening under nominal conditions (a) and disturbances (b).

this to torques would enable more complex rotational tasks, such as knob-turning or valve operation. Second, as analyzed in Sec. VI-C, the slight degradation in position accuracy when introducing force-related predictions suggests an interference between control modalities within the VLA backbone. Optimizing the injection mechanism remains an open challenge.

VII. CONCLUSION

This paper identifies the simulation dynamics gap as a conflict between the need for target force and the unreliability of simulated force magnitudes. By leveraging contact force direction as a dynamics-invariant geometric feature, we enable policy transfer using pure simulation data. Our force-aware admittance controller, paired with minimal manual tuning of target force magnitude, ensures stable contact-rich manipulation. Across four real-world tasks, our framework outperforms large-scale VLA baselines with blind-compliance controllers.

REFERENCES

[1] Malek Aburub, Cristian C Beltran-Hernandez, Tatsuya Kamijo, and Masashi Hamaya. Learning diffusion policies from demonstrations for compliant contact-rich manipulation. *arXiv preprint arXiv:2410.19235*, 2024.

[2] Kevin Black, Noah Brown, Danny Driess, Adnan Esmail, Michael Equi, Chelsea Finn, Niccolò Fusai, Lachy Groom, Karol Hausman, Brian Ichter, et al. π_0 : A vision-language-action flow model for general robot control. *arXiv preprint arXiv:2410.24164*, 2024.

[3] Jeannette Bohg, Karol Hausman, Bharath Sankaran, Oliver Brock, Danica Kragic, Stefan Schaal, and Gaurav S. Sukhatme. Interactive perception: Leveraging action in perception and perception in action. *IEEE Transactions on Robotics*, 33(6):1273–1291, 2017.

[4] Anzhe Chen, Yifei Yang, Zhenjie Zhu, Kechun Xu, Zhongxiang Zhou, Rong Xiong, and Yue Wang. Toward embodiment equivariant vision-language-action policy. *arXiv preprint arXiv:2509.14630*, 2025.

[5] Tianxing Chen, Zanxin Chen, Baijun Chen, Zijian Cai, Yibin Liu, Zixuan Li, Qiwei Liang, Xianliang Lin, Yiheng Ge, Zhenyu Gu, et al. Robotwin 2.0: A scalable data generator and benchmark with strong domain randomization for robust bimanual robotic manipulation. *arXiv preprint arXiv:2506.18088*, 2025.

[6] Hojung Choi, Yifan Hou, Chuer Pan, Seongheon Hong, Austin Patel, Xiaomeng Xu, Mark R. Cutkosky, and Shuran Song. In-the-wild compliant manipulation with umi-ft. *arXiv preprint arXiv:2601.09988*, 2026.

[7] Tan-Dzung Do, Nandiraju Gireesh, Jilong Wang, and He Wang. Watch less, feel more: Sim-to-real rl for generalizable articulated object manipulation via motion adaptation and impedance control. In *8th Annual Conference on Robot Learning (CoRL)*, 2024.

[8] Caelan Garrett, Ajay Mandlekar, Bowen Wen, and Dieter Fox. Skillmimicgen: Automated demonstration generation for efficient skill learning and deployment. In *8th Annual Conference on Robot Learning (CoRL)*, 2024.

[9] Tairan He, Zi Wang, Haoru Xue, Qingwei Ben, Zhengyi Luo, Wenli Xiao, Ye Yuan, Xingye Da, Fernando Castañeda, Shankar Sastry, Changliu Liu, Guanya Shi, Linxi Fan, and Yuke Zhu. Viral: Visual sim-to-real at scale for humanoid loco-manipulation. *arXiv preprint arXiv:2511.15200*, 2025.

[10] Zihao He, Hongjie Fang, Jingjing Chen, Hao-Shu Fang, and Cewu Lu. Foar: Force-aware reactive policy for contact-rich robotic manipulation. *IEEE Robotics and Automation Letters*, 2025.

[11] Yifan Hou, Zeyi Liu, Cheng Chi, Eric Cousineau, Naveen Kuppuswamy, Siyuan Feng, Benjamin Burchfiel, and Shuran Song. Adaptive compliance policy: Learning approximate compliance for diffusion guided control. In *2025 IEEE International Conference on Robotics and Automation (ICRA)*, 2025.

[12] Physical Intelligence, Ali Amin, Raichelle Aniceto, Ashwin Balakrishna, Kevin Black, Ken Conley, Grace Conners, James Darpinian, Karan Dhabalia, Jared DiCarlo, et al. $\pi_{0.6}^*$: A vla that learns from experience. *arXiv preprint arXiv:2511.14759*, 2025.

[13] Yunfan Jiang, Chen Wang, Ruohan Zhang, Jiajun Wu, and Li Fei-Fei. Transic: Sim-to-real policy transfer by learning from online correction. In *8th Annual Conference on Robot Learning (CoRL)*, 2024.

[14] Zhenyu Jiang, Yuqi Xie, Kevin Lin, Zhenjia Xu, Weikang Wan, Ajay Mandlekar, Linxi Fan, and Yuke Zhu. Dexmimicgen: Automated data generation for bimanual dexterous manipulation via imitation learning. In *IEEE International Conference on Robotics and Automation (ICRA)*, 2025.

[15] Abhishek Joshi, Beining Han, Jack Nugent, Max Gonzalez Saez-Diez, Yiming Zuo, Jonathan Liu, Hongyu Wen, Stamatis Alexandropoulos, Karhan Kayan, Anna Calveri, Tao Sun, Gaowen Liu, Yi Shao, Alexander Raistrick, and Jia Deng. Procedural generation of articulated simulation-ready assets, 2025.

[16] Kun Lei, Huanyu Li, Dongjie Yu, Zhenyu Wei, Lingxiao Guo, Zhennan Jiang, Ziyu Wang, Shiyu Liang, and Huazhe Xu. RI-100: Performant robotic manipulation with real-world reinforcement learning. *arXiv preprint arXiv:2510.14830*, 2025.

[17] Yu Li, Xiaojie Zhang, Ruihai Wu, Zilong Zhang, Yiran Geng, Hao Dong, and Zhaofeng He. Unidoormanip: Learning universal door manipulation policy over large-scale and diverse door manipulation environments. *arXiv preprint arXiv:2403.02604*, 2024.

[18] Wenhui Liu, Junbo Wang, Yiming Wang, Weiming Wang, and Cewu Lu. Forcemimic: Force-centric imitation learning with force-motion capture system for contact-rich manipulation. In *2025 IEEE International Conference on Robotics and Automation (ICRA)*, 2025.

[19] Jianlan Luo, Charles Xu, Jeffrey Wu, and Sergey Levine. Precise and dexterous robotic manipulation via human-in-the-loop reinforcement learning. *Science Robotics*, 10(105):eads5033, 2025.

[20] Ajay Mandlekar, Soroush Nasiriany, Bowen Wen, Iretiayo Akinola, Yashraj Narang, Linxi Fan, Yuke Zhu, and Dieter Fox. Mimicgen: A data generation system for scalable robot learning using human demonstrations. In *7th Annual Conference on Robot Learning (CoRL)*, 2023.

[21] James Tigue Mayank Mittal, Pascal Roth et al. Isaac lab: A gpu-accelerated simulation framework for multi-modal robot learning. *arXiv preprint arXiv:2511.04831*, 2025.

[22] Marius Memmel, Andrew Wagenmaker, Chunling Zhu, Dieter Fox, and Abhishek Gupta. ASID: Active exploration for system identification in robotic manipulation. In *The Twelfth International Conference on Learning Representations (ICLR)*, 2024.

[23] Yao Mu, Tianxing Chen, Zanxin Chen, Shijia Peng, Zhiqian Lan, Zeyu Gao, Zhixuan Liang, Qiaojun Yu, Yude Zou, Mingkun Xu, Lunkai Lin, Zhiqiang Xie, Mingyu Ding, and Ping Luo. Robotwin: Dual-arm robot

benchmark with generative digital twins. In *Proceedings of the Computer Vision and Pattern Recognition Conference (CVPR)*, 2025.

[24] Michael Noseworthy, Bingjie Tang, Bowen Wen, Ankur Handa, Chad Kessens, Nicholas Roy, Dieter Fox, Fabio Ramos, Yashraj Narang, and Iretiayo Akinola. Forge: Force-guided exploration for robust contact-rich manipulation under uncertainty. *IEEE Robotics and Automation Letters*, 10(5):4436–4443, 2025.

[25] NVIDIA. Isaac Sim. URL <https://github.com/isaac-sim/IsaacSim>.

[26] Marcel Torne Villasevil, Anthony Simeonov, Zechu Li, April Chan, Tao Chen, Abhishek Gupta, and Pulkit Agrawal. Reconciling reality through simulation: A real-to-sim-to-real approach for robust manipulation. In *Proceedings of Robotics: Science and Systems (RSS)*, 2024.

[27] Yilin Wang, Shangzhe Li, Haoyi Niu, Zhiao Huang, Weitong Zhang, and Hao Su. A recipe for efficient sim-to-real transfer in manipulation with online imitation-pretrained world models. *arXiv preprint arXiv:2510.02538*, 2025.

[28] Haoyu Xiong, Russell Mendonca, Kenneth Shaw, and Deepak Pathak. Adaptive mobile manipulation for articulated objects in the open world. *arXiv preprint arXiv:2401.14403*, 2024.

[29] Xiaomeng Xu, Yifan Hou, Zeyi Liu, and Shuran Song. Compliant residual DAgger: Improving real-world contact-rich manipulation with human corrections. In *The Thirty-ninth Annual Conference on Neural Information Processing Systems (NeurIPS)*, 2025.

[30] Zhenjia Xu, Jiajun Wu, Andy Zeng, Joshua B Tenenbaum, and Shuran Song. Densephysnet: Learning dense physical object representations via multi-step dynamic interactions. In *Proceedings of Robotics: Science and Systems (RSS)*, 2019.

[31] Han Xue, Jieji Ren, Wendi Chen, Gu Zhang, Yuan Fang, Guoying Gu, Huazhe Xu, and Cewu Lu. Reactive diffusion policy: Slow-fast visual-tactile policy learning for contact-rich manipulation. In *Proceedings of Robotics: Science and Systems (RSS)*, 2025.

[32] Haoru Xue, Tairan He, Zi Wang, Qingwei Ben, Wenli Xiao, Zhengyi Luo, Xingye Da, Fernando Castañeda, Guanya Shi, Shankar Sastry, Linxi "Jim" Fan, and Yuke Zhu. Opening the sim-to-real door for humanoid pixel-to-action policy transfer. *arXiv preprint arXiv:2512.01061*, 2025.

[33] Yifei Yang, Lu Chen, Zherui Song, Yenan Chen, Wentao Sun, Zhongxiang Zhou, Rong Xiong, and Yue Wang. Disambiguate gripper state in grasp-based tasks: Pseudo-tactile as feedback enables pure simulation learning. In *IEEE International Conference on Intelligent Robots and Systems (IROS)*, 2025.

[34] Patrick Yin, Tyler Westenbroek, Simran Bagaria, Kevin Huang, Ching-An Cheng, Andrey Kolobov, and Abhishek Gupta. Rapidly adapting policies to the real-world via simulation-guided fine-tuning. In *CoRL 2024 Workshop on Mastering Robot Manipulation in a World of Abundant Data*, 2024.

[35] Jiawen Yu, Hairuo Liu, Qiaojun Yu, Jieji Ren, Ce Hao, Haitong Ding, Guangyu Huang, Guofan Huang, Yan Song, Panpan Cai, Wenqiang Zhang, and Cewu Lu. ForceVLA: Enhancing VLA models with a force-aware moe for contact-rich manipulation. In *The Thirty-ninth Annual Conference on Neural Information Processing Systems (NeurIPS)*, 2025.

[36] Zongzheng Zhang, Haobo Xu, Zhuo Yang, Chenghao Yue, Zehao Lin, Huan-ang Gao, Ziwei Wang, and Hao Zhao. Elucidating the design space of torque-aware vision-language-action models. In *9th Annual Conference on Robot Learning (CoRL)*, 2025.

[37] Yi Zhou, Connelly Barnes, Jingwan Lu, Jimei Yang, and Hao Li. On the continuity of rotation representations in neural networks. In *2019 IEEE/CVF Conference on Computer Vision and Pattern Recognition (CVPR)*, 2019.

APPENDIX

A. Observation Specification

The observation O_t captures the geometric state of the environment through visual and proprioceptive modalities:

- Vision (I_t): A set of RGB images captured from multi-view cameras, including one wrist-mounted view for fine alignment and 1-2 fixed third-person views for global context.
- Proprioception ($X_t \in \mathbb{R}^{10}$): A vector containing the end-effector position (3), the 6D rotation (6) proposed in [37], and the gripper state (1).

B. Task-Specific Kinematic Rules

In *Contact Interaction* phases, the feasible motion is constrained by the object's geometry and physical mechanism. The expert FSM generates pose trajectories based on the specific kinematic constraints of each task:

- Peg-in-hole: A trajectory descending vertically along the central axis of the hole after the peg and hole are aligned.
- Whiteboard Wiping: A zigzag trajectory covering the ink area while aligning with the surface normal, generated using a heuristic coverage path planning algorithm.
- Articulated Objects (Door/Microwave): An ideal circular trajectory around the joint axis, computed analytically using Rodrigues' rotation formula based on the ground-truth joint axis and pivot point from the simulator.

C. Simulation Environments Construction

To enable successful transfer of the policy to the real world, non-dynamic sim-real discrepancies must also be minimized. Accordingly, we construct simulation environments to reduce visual and geometric gaps, while ensuring the fidelity of interaction logic.

1) *High-Fidelity Assets*: For objects with complex textures or geometries, we use off-the-shelf scanning apps (e.g., RealityComposer) to generate textured 3D meshes and post-process them in Blender to separate movable components. These assets are then rigged in Isaac Sim [25] to match the real-world kinematics. However, for the Peg-in-hole task, where millimeter precision is critical, we utilize high-precision CAD assets in simulation and manufacture the physical peg and hole using 3D printing.

2) *High-Fidelity Interaction Logic*: Beyond texture and geometry, we explicitly model the interaction logic to prevent the policy from learning incorrect causal relationships (e.g., pulling a door without unlatching).

- Ink Removal: For the whiteboard wiping task, we simulate the physical erasure process using a dynamic transparency masking technique, where visual elements turn transparent based on the eraser's proximity.
- Door Locking: For the door opening task, we simulate the mechanical latch by applying a conditional external force field that actively resists the door opening motion. This resistance is disengaged only when the handle rotation exceeds a threshold, enforcing the correct "turn-then-pull" manipulation sequence.

The photorealistic assets minimize the visual and geometric gap, while the precise interaction logic ensures the policy learns valid physical manipulation skills rather than exploiting simulation artifacts.

D. Randomization Strategy

To ensure robust sim-to-real transfer, we apply extensive randomization to the non-dynamic aspects of the environment:

- Initial State Randomization: the object's pose and the robot's initial configuration.
- Visual Randomization: lighting conditions, background scenes, and the cameras' intrinsics and extrinsics.

Notably we do *not* randomize dynamic parameters, because the policy is explicitly formulated to be invariant to dynamic.

E. Parameter Selection Principles for Admittance Controller

The virtual mass m is fixed, while the stiffness k is set to relatively low values to provide passive compliance and mitigate the impact of prediction errors during contact. The damping is set as $d = 2\xi\sqrt{mk}$ with over-damped ratio $\xi = 2$, to improve stability and suppresses oscillations in practice.

F. Finetuning Strategy

To preserve the benefits of pre-training, we adopt a selective initialization strategy: projection weights corresponding to the original action dimensions are inherited from the pre-trained model, while those associated with newly introduced dimensions are initialized with small magnitudes. This keeps the initial policy behavior close to the pre-trained model, stabilizing finetuning.

G. Proof of Propositions in Section V-B

We model the environment as a linear spring with stiffness k_e and denote the rest point of the environment as x_e . The external force can then be expressed as

$$f_{ext,n} = k_e(x_e - x_n), \quad (7)$$

where x_n is the end-effector position along the normal direction n . Note that m, d, k_e, f_H are all positive and constant.

1) **Proposition 1**: *Under disturbance-free conditions, the closed-loop normal-direction dynamics is asymptotically stable and converges to the equilibrium point $x_n = x_e - f_H/k_e$ such that $f_{ext,n} = f_H$.*

Proof. Under disturbance-free conditions, x_e is constant. Substituting Eq. 7 into Eq. 4 yields the closed-loop dynamics:

$$m\ddot{x}_n + 2d\dot{x}_n = k_e(x_e - x_n) - f_H. \quad (8)$$

We define the error state as $e = x_n - (x_e - f_H/k_e)$ and rewrite Eq. 8 as

$$m\ddot{e} + 2d\dot{e} + k_e e = 0. \quad (9)$$

Let $V(e, \dot{e}) = \frac{1}{2}m\dot{e}^2 + \frac{1}{2}k_e e^2$ be a candidate Lyapunov function, which is positive definite. Its time derivative is $\dot{V}(e, \dot{e}) = -2d\dot{e}^2 \leq 0$. According to LaSalle's invariance principle, the system converges to the largest invariant set where $\dot{V} = 0$, i.e., $\dot{e} = 0$, and thus $\ddot{e} = 0$. Within this set, Eq. 9 implies $e = 0$. Therefore, the closed-loop system is

asymptotically stable and converges to $x_n = x_e - f_H/k_e$, which satisfies $f_{ext,n} = f_H$ according to Eq. 6. \square

2) **Proposition 2:** When contact with the environment is lost due to an external disturbance (e.g., lowering the whiteboard during wiping), the closed-loop normal-direction dynamics are asymptotically stable in velocity. Specifically, the end-effector velocity converges to the steady-state value $\dot{x}_n = -\frac{f_H}{2d}$, which drives the robot toward the environment to facilitate contact re-establishment.

Proof. When the robot loses contact, $f_{ext,n} = 0$. Substituting this into Eq. 4 yields

$$m\ddot{x}_n + 2d\dot{x}_n = -f_H. \quad (10)$$

We define velocity error as $e_v = \dot{x}_n + \frac{f_H}{2d}$ and rewrite Eq. 10:

$$m\dot{e}_v + 2de_v = 0. \quad (11)$$

Let $V(e_v) = \frac{1}{2}me_v^2$ be a candidate Lyapunov function, which is positive definite. Its time derivative is $\dot{V}(e_v) = -2de_v^2 \leq 0$. According to LaSalle's invariance principle, the system converges to the largest invariant set where $\dot{V} = 0$, i.e., $e_v = 0$. Therefore, the closed-loop system is asymptotically stable in terms of velocity and converges to $\dot{x}_n = -\frac{f_H}{2d}$. Note that while the position x_n evolves linearly due to the velocity, this behavior is intentional, as it drives the end-effector toward the environment to re-establish contact. \square

3) **Proposition 3:** When the disturbance occurs during contact, the closed-loop normal-direction dynamics is input-to-state stable (ISS) with respect to the disturbance.

Proof. When a disturbance occurs during contact, x_e becomes time-varying. The closed-loop dynamics is the same as Eq. 8, which can be rewritten in terms of the error state $e = x_n - (x_e - f_H/k_e)$ as

$$m\ddot{e} + 2d\dot{e} + k_e e = u, \quad (12)$$

where $u = -(m\ddot{x}_e + 2d\dot{x}_e)$ represents the bounded disturbance input. We choose the same candidate Lyapunov function as in Proposition 1, $V(e, \dot{e}) = \frac{1}{2}m\dot{e}^2 + \frac{1}{2}k_e e^2$. Its time derivative is

$$\dot{V}(e, \dot{e}) = -2d\dot{e}^2 + \dot{e}u. \quad (13)$$

Using Young's inequality, we have $\dot{e}u \leq d\dot{e}^2 + \frac{u^2}{4d}$. Substituting this into Eq. 13 yields

$$\dot{V}(e, \dot{e}) \leq -d\dot{e}^2 + \frac{u^2}{4d}. \quad (14)$$

This implies that when $\|\dot{e}\| \geq \frac{|u|}{2d}$, $\dot{V}(e, \dot{e}) \leq 0$. Therefore, the closed-loop system is input-to-state stable (ISS) with respect to the disturbance u . This indicates that the system can maintain bounded states (i.e. e and \dot{e}) in the presence of bounded disturbances. \square

H. Platform

Figure 7 shows our real-world experimental platform, consisting of a Franka Panda robot arm with a Franka Hand gripper, a wrist-mounted Intel RealSense D435 camera, and 2 fixed third-person RealSense D435 cameras. The whiteboard wiping task uses all three cameras, while the other tasks utilize only the “Wrist Camera” and “Third-View Camera 1”.

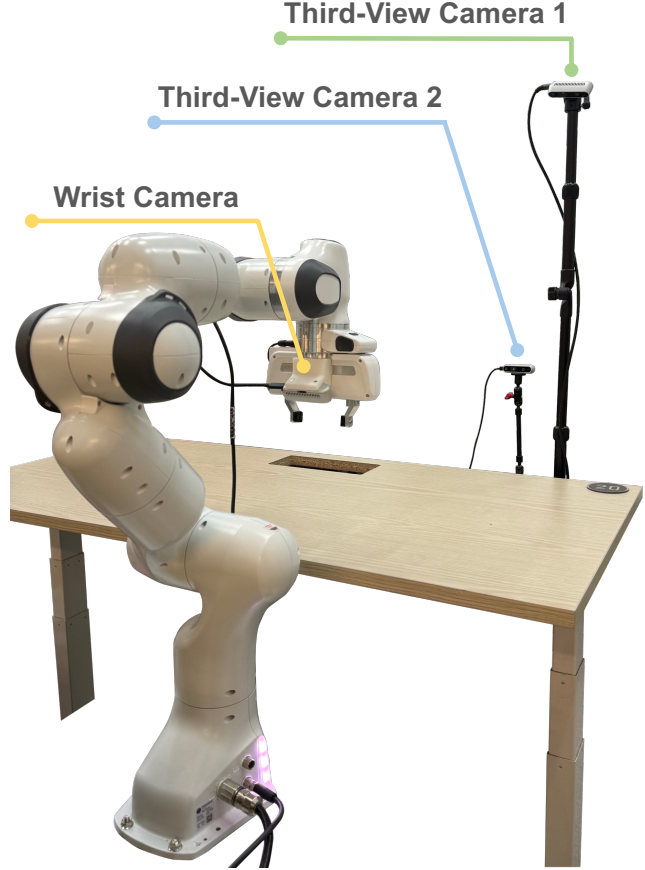


Fig. 7. Real-world platform.

I. Task Description

We evaluate our framework on four contact-rich manipulation tasks:

Microwave Opening (MO). Opening a microwave door by grasping the handle and pulling it open. This task requires overcoming resistive forces from the snap lock, while contact is primarily maintained by the gripper.

Peg-in-Hole (PH). Insert a cylindrical peg into a hole with a clearance of about 1mm. The ultimate goal is to bring the peg into contact with the bottom of the hole, thus demands normal force to secure the insertion depth. In the tangent direction, there is no resistance to overcome, and compliance is the primary objective.

Whiteboard Wiping (WW). Wipe off ink from a whiteboard surface using an eraser. This task requires normal force to maintain contact between the eraser and whiteboard, ensuring effective wiping. Additionally, the robot must overcome friction during wiping motions.

Door Opening (DO). Open a door by first turning the handle and then pulling the door open. This task involves constraint switching, as the manifold constraint changes from the handle rotation to the door pulling. In the first phase (handle turning), the robot must overcome the spring resistance of the latch. In the second phase (door pulling), the robot needs to counteract

frictional forces. Contact is maintained by the gripper closure.

J. Details of Evaluation Protocols

The object pose randomization ranges, disturbance protocols, and success criteria for each task are as follows:

Microwave Opening. The microwave is randomly placed on a table within a $10\text{cm} \times 20\text{cm} \times 10\text{cm}$ area, with random orientations around the vertical axis within $\pm 15^\circ$. Disturbances are introduced by having the human evaluator apply random forces to the microwave during the door-opening process. The task is considered successful if the door is opened to at least 50° within 120 seconds.

Peg-in-Hole. The hole is randomly placed on a table within a $40\text{cm} \times 40\text{cm} \times 20\text{cm}$ area, with random orientations around the vertical axis within $\pm 90^\circ$. The human evaluator raises, lowers, or horizontally moves the hole to apply disturbances after partial insertion of the peg. The depth of the hole is 25mm, and the task is considered successful if the peg is inserted to at least 10mm within 60 seconds.

Whiteboard Wiping. The whiteboard is placed in a fixed location on a table, with random height adjustments within 10cm and random orientations around the x-axis within $\pm 20^\circ$. The human evaluator writes random scribbles on the whiteboard before each trial and keeps the shape and location of the scribbles similar across all methods. The disturbances are applied during wiping: raising, lowering, tilting, or horizontally moving the whiteboard. The task is considered successful if the remaining ink is less than 5cm within 120 seconds.

Door Opening. The door is randomly placed within a $10\text{cm} \times 30\text{cm} \times 10\text{cm}$ area, with random orientations around the vertical axis within $\pm 15^\circ$. The disturbances are introduced by applying random forces to the door during the handle-turning and door-pulling phases. The task is considered successful if the door is opened to at least 30° within 120 seconds.

K. Additional Implementation Details

We collect 2000 demonstrations in IsaacLab [21] for each task and train one policy per task. The training settings for all baselines follow those reported in the original papers. Our method uses the same setting as E2VLA. The execution horizon for all methods is set to 16 steps with 10 FPS. The controller operates at 1000 Hz. For the controller parameters, we set the damping ratio $\xi = 2$. The rotational mass is set to 0.1 with stiffness 10. The translational mass is set to 1.0. For baselines, the low/mid/high stiffness values are set to 50/200/800. For our method, the translational stiffness is set to 50. For all controllers, we apply a force and torque deadband of 2N and 1Nm, respectively, to suppress small-magnitude oscillations and ensure stable execution.